optica

Dispersion engineering of crystalline resonators via microstructuring: supplementary material

IVAN S. GRUDININ* AND NAN YU

Jet Propulsion Laboratory, California Institute of Technology, 4800 Oak Grove Dr., Pasadena, California 91109, USA

**Corresponding author: grudinin@jpl.nasa.gov*

Published 4 March 2015

This document provides supplementary material to "Dispersion engineering of crystalline resonators via microstructuring," http://dx.doi.org/10.1364/optica.2.000221. Record quality factors and large selection of materials make optical crystalline resonators attractive for emerging areas of research. While basic parameters of a resonator are important, fine-tuning of its mode frequencies can dramatically improve efficiency of nonlinear optical interactions. However, dispersion engineering of high quality crystalline resonators has not been reported due to limitations of existing methods. Moreover, spectral and dispersion engineering often can not be effectively combined in demonstrated approaches. Here we show by numerical modeling that dispersion can be engineered by micro-structuring the light-guiding boundary of a resonator that is built around an axially symmetric substrate. We experimentally demonstrate ultrahigh-quality-factor (1×10^8) crystalline resonators capable of generating Kerr combs with expanded bandwidth. The new approach enables spectral and dispersion engineering flexibility in any resonator with axial symmetry that can support a photonic belt structure. In this supplementary material we present more details to support our claims.

http://dx.doi.org/10.1364/optica.2.000221.s001

1. FREQUENCY COMBS FROM THE PHOTONIC BELT RESONATORS

We have carried out initial studies of frequency comb formation observed in several PBRs shown in Fig. S1. The FEM modeling of the fabricated resonators requires knowledge of their cross sections. Such images could not be obtained by optical microscopy or profilometry due to insufficient resolution. The electron microscopy requires a metal coating to counter charging effects, thus making the resonator unusable. We obtained the cross section images with sub-wavelength resolution nondestructively by using a new technique. We start by making a resin cast of a resonator by direct contact and lift–off. The cast is then filled with a glue having different refractive index from the cast material. After hardening, the replica can be cut and polished to reproduce the resonator cross section. Optical microscope is then used to obtain the image of the resonator boundary.

Since the values of D_2 are around 10 kHz for resonator sizes used in this work, we find the eigenfrequencies f_{l-1}, f_l, f_{l+1} with around 1 kHz precision to minimize the error of derived GVD. Typically, the required eigenvalue precision is achieved with meshes containing up to 0.5 million elements. To handle such meshes we implemented our solver on multiple processors of a shared memory parallel computer using the message passing interface coding. To obtain each eigenfrequency we start with an approximate set of parameters and a rough mesh. The mesh is then refined and adapted to each intermediate solution. The refractive indices are updated with the Sellmeier equations at each step and the birefringence is taken into account. This iterative refining procedure is repeated until the eigenvalue converges with desired precision. The FEM solver was verified by comparing its results with the eigenvalues for a spherical resonator[1], for which the exact solutions can be obtained. We used Koheras Adjustik fiber laser with 20 kHz short-term linewidth around λ=1561 nm to pump the blue side of the resonance curve for frequency comb generation. The pump power was amplified with an IPG Photonics EDFA and fixed at 300 mW, while the actual power coupled to the resonator is given by the coupling efficiency. Both res-

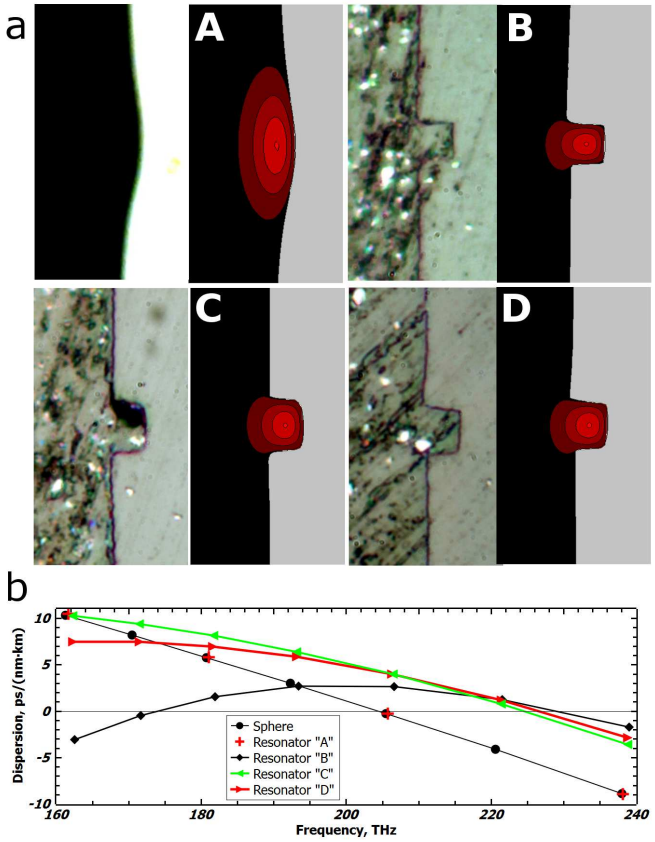

Fig. S1. Optical resonators and corresponding dispersion. **a**, Each of the 8 images represents an area sized 25 × 45 micrometers. The optical images of the resonator cross sections obtained with the new technique are shown along with the mode intensity maps produced by FEM modeling. **b**, Numerically computed total GVD for the resonators shown in a). The resonator A with Gaussian boundary shape has the same dispersion as an ideal sphere.

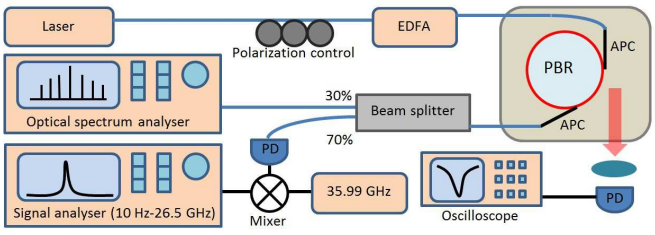

Fig. S2. Schematics of experimental setup. Pump laser is used to excite the TE mode of a PBR. EDFA — erbium doped fiber amplifier, PD — photodetector, APC — angle polished fiber coupler.

onators A and B have FSR of 46 GHz, loaded Q of 60 million and critical coupling of around 70%. As the detuning was reduced from the blue side we observed previously reported comb formation dynamics[2, 3] with some new features (see Fig.S3). The schematics of the experimental setup is shown in Fig. S2. The comb was detected with optical spectrum analyzers Yokogawa AQ6319 and AQ6375. We also detected the comb on a fast photodetector (New Focus 1014) to measure the beatnote between different comb frequencies. The optical Q was measured by means of a sideband modulation technique. The comb in PBR B is a three–staged comb in contrast to primary–secondary combs observed in all other reported resonators to the best of our knowledge. The primary comb starts with two sidebands separated by $N \times FSR$, where N is integer. The secondary comb is still spaced by a multiple of resonator's FSR, whereas the third stage of comb formation fills the FSR–spaced resonator modes. In all of the resonators shown in Fig. S1 we observed discrete transitions between the modulation instability (MI) states of the primary comb. The appearance of each new sideband pair is accompanied by reduction of N by unity and the overall growth of the primary comb span. These discrete steps eventually lead to transitional comb states [4], followed by a number of discrete transitions between stable and spectrally symmetric comb states. These final discrete transitions are also observed in resonator transmission in similarity to the steps observed on the nonlinear resonant curve during soliton formation [5, 6]. The discrete steps to the final states are observed in both two and three stage combs, whereas the three stage comb shown in Fig.S3 is not symmetric. To explore this asymmetry we performed a wider scan of the comb spectrum and discovered that the comb lines span across more than one octave in frequency as shown in Fig. S4. In this case the intrinsic Q of PBR "C" has been reduced to 50 million and the pump power after EDFA was 600 mW. It is likely that the lines near 125 THz are also present in Fig.S3, but were not detected because the absence of lines below 160 THz was assumed to be the end of the comb envelope. This absence of lines could be explained by absorption in the fibers used to route the comb to the OSA. For example, the OH group in silica is known to have strong bands in the 130–140 and 215–243 THz range [7]. Dispersion and spectrum of a particular resonator could be another reason for this window in the comb envelope. We observed broad and multiple beatnotes [3] typically spanning nearly 10 MHz around the central frequency of 45.94 GHz. The beatnote sometimes narrowed as shown in Fig. S4 inset. However, significant ripples in our EDFA output power destabilized the comb beatnote. To the best of our knowledge, this measurement represents the first octave spanning comb with repetition rate below 50 GHz and pump power of less than 1 Watt. While this initial study has not produced a coherent comb state, the purpose of these observations is to show the increase in the comb bandwith as a result of the new dispersion engineering method. The resonator and coupling parameters are summarized in Table S1. Interestingly, we found that in addition to flattened dispersion, the PBRs support only one fundamental mode family of TE polarization. Higher order TE modes are not observable at least to the detector noise level, in accordance with theory [8]. The quality factor of the fundamental TM mode family is at least 20 times lower for PBRs compared to TE modes. This could be ex-plained by the same geometric effect of mode leaking into the substrate that enables WGM single mode resonators [8, 9] sim-ilar to resonator A where we also observed the difference in Q factors experimentally. However, we found that the difference in

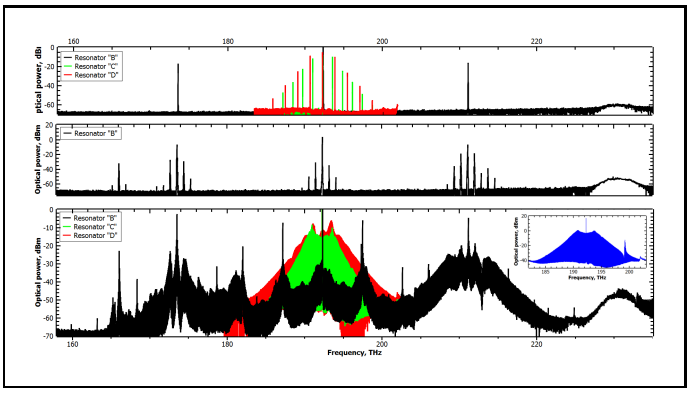

Fig. S3. Frequency combs generated in micro–structured resonators with 300 mW of pump at λ =1560 nm (192.4 THz). a, The primary comb in waveguide B starts at N=408 in contrast to N≃30 in waveguides A, C and D. **b**, Secondary comb formation in waveguide B starts as the laser detuning is reduced. **c**, Comb states at a minimum stable detuning. The comb from the waveguide B contains nearly 2000 lines spanning 100 THz and spaced by cavity FSR. Insets show cavity FSR–spaced comb lines produced by resonator A.

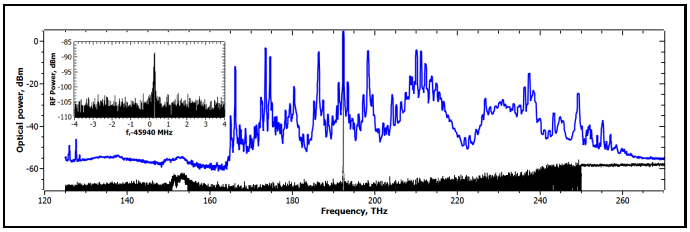

Fig. S4. Octave spanning frequency comb and its beatnote. Waveguide "C" produced comb lines spanning across over one octave (blue). The noise level for large laser detuning where no comb is generated is also shown (black). The gap could be explained by near-IR fiber absorption or by particular resonator dispersion and spectrum. Resonator intrinsic Q=50 million, pump power 600 mW.

Table S1. Parameters of resonators and combs. Quality factor of resonator "A" was reduced from the critically coupled value of 400×10^6 by overloading the output coupler. Loaded Q and cold coupling efficiency are the parameters measured at reduced pump power before and after comb generation. Intrinsic Q was derived from the linewidth measurements in critically coupled setting. (*) loaded cold / intrinsic. (**) cold/critical.

	Q*, million	Coupling**,%	N	FSR, GHz
A	69/800	38/83	29	46.06
B	58/90	21/70	408	46.05
C	61/69	21/73	29	45.96
D	36/60	15/65	31	45.96

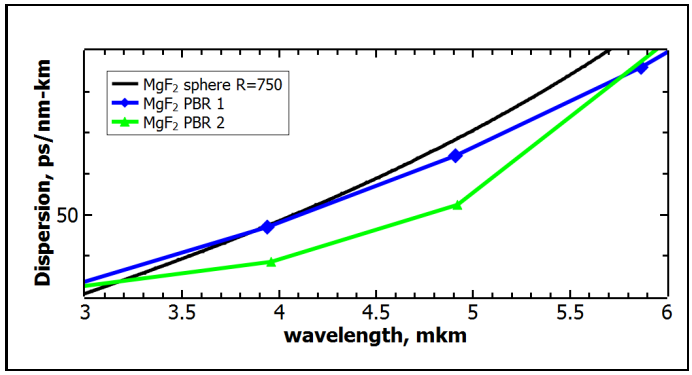

Fig. S5. Dispersion engineering in mid–IR range. Dispersion of two arbitrary MgF_2 PBRs are shown along with that of a spherical resonator.

mode field distribution between TE and TM modes in our resonators is seemingly too small to account for such a Q difference. Alternatively, the difference between the TE and TM mode Q can be explained by the same mechanism as in planar ridge waveguides, where such difference is also observed. Amore detailed theory of crystalline microresonators explaining this and other observed phenomena [10] needs to be developed.

2. FLEXIBILITY AND LIMITATIONS OF DISPERSION ENGINEERING

We have numerically investigated dispersion engineering for resonators having different dimensions and made with various materials as well as in different wavelength ranges. For exam-ple, dispersion can also be engineered in the mid–IR range as shown in Fig. S5 Our dispersion engineering approach allowed us to achieve anomalous and flattened GVD in a CaF2 PBR at wavelengths around 1550 nm. Notably, the dispersion is normal at this wavelength without dispersion engineering. With dispersion engineering, the GVD of a CaF2 resonator starts to resemble that of a spherical MgF2 resonator as shown in Fig. S6 Thus, fluorite resonators can be used for both normal and anomalous regime comb generation in the telecom band. We also fabricated two CaF_2 PBRs with different geometries and experimentally found that comb generation regimes in such resonators are strikingly different from those in the non–micro–structured resonator [11] as shown in Fig. S7. While no quantitative theory of dispersion engineering exists, we can explain the change in dispersion by the crossing between the WGMs of cylindrical substrate and the waveguide modes corresponding to the microstructured resonator boundary. Still, disper-sion of a standalone cylinder and a photonic belt are strikingly different from that of a composite PBR structure. For the longer wavelengths, the dispersion change is limited by the fact that the mode field becomes significantly larger than the photonic belt. Along the same lines, for the shorter wavelengths the mode filed becomes significantly smaller than the belt structure. Higher order micro-structuring could thus be used to extend the wavelength span of engineered dispersion for any given resonator.

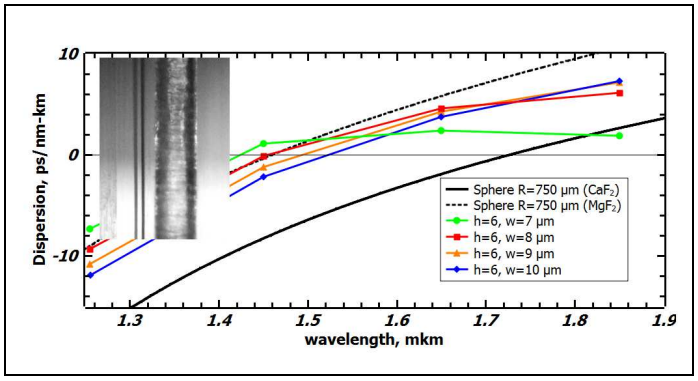

Fig. S6. Dispersion engineering in CaF_2 resonators. Fluorite PBR can be engineered to have anomalous and flat GVD in telecom range. The inset shows the PBR light-guiding structure along with the human hair approximately 50 micrometers in diameter.

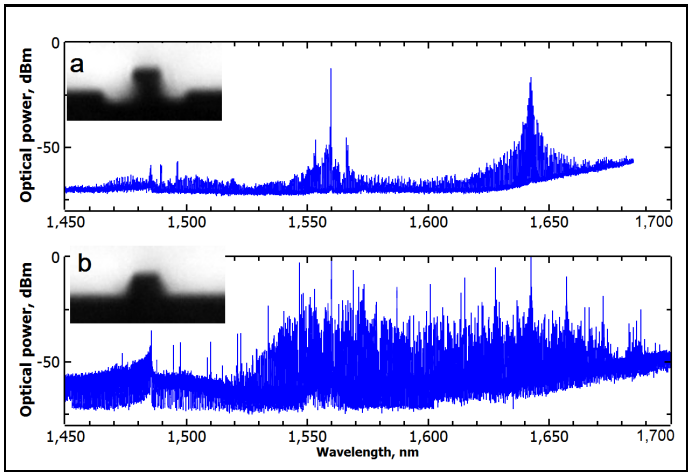

Fig. S7. Comb produced by fluorite PBR with different geometry of the light-guiding boundary The combs were obtained by scanning the laser over the resonance multiple times and averaging the output. Pump power is around 100 mW.

REFERENCES

1. I. S. Grudinin and N. Yu, J. Opt. Soc. Am. B **29**, 3010–3014 (2012).
2. Y. K. Chembo, D. V. Strekalov, and N. Yu, Phys. Rev. Lett. **104**, 103902 (2010).
3. T. Herr, K. Hartinger, J. Riemensberger, C. Y. Wang, E. Gavartin, R. Holzwarth, M. L. Gorodetsky, and T. J. Kippenberg, Nat. Photonics **6**, 480–487 (2012).
4. S. Coen and M. Erkintalo, Opt. Lett. **38**, 1790–1792 (2013).
5. T. Herr, V. Brasch, J. D. Jost, C. Y. Wang, N. M. Kondratiev, M. L. Gorodetsky, and T. J. Kippenberg, Nat. Photonics **8**, 145–152 (2014).
6. T. Herr, V. Brasch, J. D. Jost, I. Mirgorodskiy, G. Lihachev, M. L. Gorodetsky, and T. Kippenberg, Phys. Rev. Lett. **113**, 123901 (2014).
7. C. R. Elliott and G. R. Newns, Appl. Spectrosc. **25**, 378–379 (1971).
8. A. A. Savchenkov, I. S. Grudinin, A. B. Matsko, D. Strekalov, M. Mohageg, V. S. Ilchenko, , and L. Maleki, Opt. Lett. **31**, 1313–1315 (2006).
9. F. Ferdous, A. A. Demchenko, S. P. Vyatchanin, A. B. Matsko, and L. Maleki, Phys. Rev. A **90**, 033826 (2014).
10. I. S. Grudinin, N. Yu, and L. Maleki, Opt. Lett **34**, 878–880 (2009).
11. I. S. Grudinin, G. Lin, and N. Yu, Opt. Lett **38**, 2410–2412 (2013).